Bioresource Technology 235 (2017) 1–11

Contents lists available at ScienceDirect

Bioresource Technology

journal homepage: www.elsevier.com/locate/biortech

A comprehensive kinetics study of coconut shell waste pyrolysis

Imtiaz Ali [a,*], Haitham Bahaitham [b], Raed Naebulharam [b]

[a] Department of Chemical and Materials Engineering, King Abdulaziz University, Rabigh, Saudi Arabia
[b] Department of Industrial Engineering, King Abdulaziz University, Rabigh, Saudi Arabia

HIGHLIGHTS

- Integral model-fitting methods are more accurate for one-step reaction mechanism.
- $f(\alpha) = (1-\alpha)^4 \cdot [-\ln(1-\alpha)]^{0.53}$ is the reaction model of CSW pyrolysis.
- Four independent-parallel-reaction model fits well with Gaussian distributions.
- E_a of pseudo-components can be reliably estimated from model-free methods.

GRAPHICAL ABSTRACT

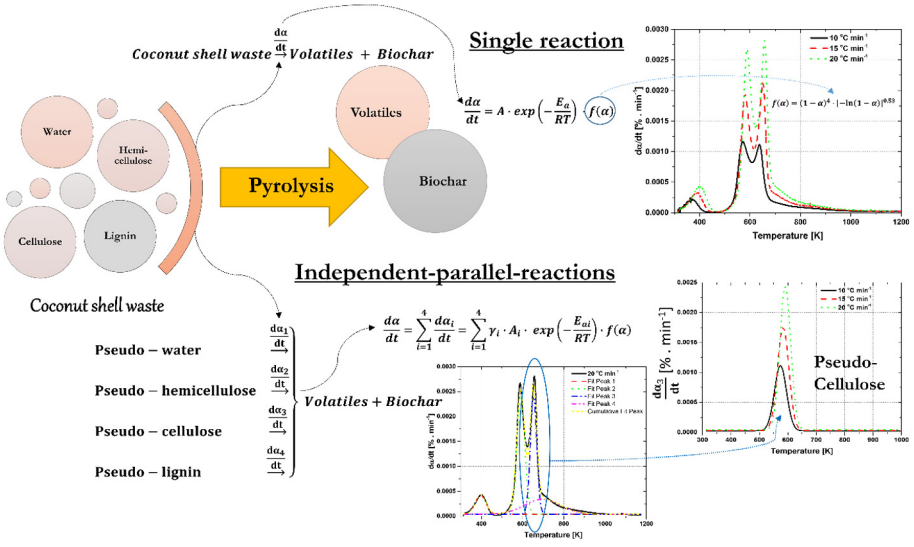

ARTICLE INFO

Article history:
Received 20 February 2017
Received in revised form 13 March 2017
Accepted 14 March 2017
Available online 18 March 2017

Keywords:
Coconut shell waste
Pyrolysis
Iso-conversional methods
Pseudo-components
Independent parallel reactions

ABSTRACT

Model-free and model-fitting methods were compared for pyrolytic conversion of the coconut shell waste. The apparent activation energy, estimated from differential and integral iso-conversional methods, increased with the progression of pyrolytic conversion. The reaction model, $f(\alpha) = (1-\alpha)^4 \cdot [-\ln(1-\alpha)]^{0.53}$, indicate that order-based nucleation and growth mechanisms control the solid-state pyrolysis of the coconut shell waste. The active pyrolysis zone was consisted of overlapping multi-component degradation peaks. Average activation energy of the pseudo-components estimated from the Kissinger's method were 21.9 kJ.mol^{-1}, 106.4 kJ.mol^{-1} and 108.6 kJ.mol^{-1} for the dehydration, the degradation of pseudo-cellulose and pseudo-hemicellulose, respectively. Pseudo-lignin decomposed over a wide range of temperature with a slower conversion rate as compared to pseudo-hemicellulose and pseudo-cellulose. Average activation energy range of pseudo-lignin was estimated from the combination of model-free and model-fitting methods as 79.1–226.5 kJ.mol^{-1}.

1. Introduction

Modern society is struggling to meet the growing demand of energy. The non-renewable fossil fuel reserves are depleting, their

* Corresponding author.
E-mail address: imtiaz_che@hotmail.com (I. Ali).

http://dx.doi.org/10.1016/j.biortech.2017.03.089
0960-8524/

Nomenclature

ASTM	American Society for Testing and Materials
CSW	Coconut Shell Waste
DTG	Differential Thermogravimetric Analysis
FWO	Flynn-Wall-Ozawa
GRG	Generalized Reduced Gradient
HHV	Higher Heating Value
IPR	Independent Parallel Reaction
KAS	Kissinger-Akahira-Sunose
LMA	Levenberg-Marquardt algorithm
P-C	Pseudo-cellulose
P-H	Pseudo-hemicellulose
P-L	Pseudo-lignin
P-W	Pseudo-water
SB	Šesták and Berggren
TG	Thermogravimetric Analysis
TGA	Thermogravimetric Analyzer
E_a	Activation energy [kJ·mol^{-1}]
E_α	Apparent activation energy [kJ·mol^{-1}]
R^2	Coefficient of determination [–]
α	Conversion [–]
$\frac{d\alpha}{dt}$	Conversion rate [s^{-1}]
$\left(\frac{d\alpha}{dt}\right)_{\alpha i}$	Conversion rate at a particular degree of conversion (α_i) [s^{-1}]
$\left(\frac{d\alpha}{dt}\right)_{pi}$	Maximum conversion rate [s^{-1}]
$\left(\frac{d\alpha}{dt}\right)_p$	Maximum value of $\frac{d\alpha}{dt}\|_{exp}$ [s^{-1}]
$\frac{d\alpha}{dt}\|_{exp}$	Experimental conversion rate [s^{-1}]
$\frac{d\alpha}{dt}\|_{pred}$	Predicted conversion rate from model equation [s^{-1}]
β	Heating rate [K · s^{-1}]
m_0	Initial mass [kg]
m_i	Instantaneous mass [kg]
m_f	Final mass [kg]
γ_i	Mass loss contribution of a pseudo-component [–]
ϑ	Degree of freedom [–]
N	Number of pseudo-components [–]
OF	Objective function [s^{-2}]
A	Pre-exponential factor [s^{-1}]
A_α	Pre-exponential factor at α_i [s^{-1}]
$f(\alpha)$	Reaction model
n	Reaction order [–]
χ^2_{red}	Reduced chi square [–]
m, p	SB model parameters [–]
T	Temperature [K]
$T_{\alpha i}$	Temperature at α_i [K]
T_{pi}	Peak-maximum temperature at $\left(\frac{d\alpha}{dt}\right)_{pi}$ [K]
R	Universal gas constant [8.314 J · mol^{-1} · K^{-1}]
σ^2	Variance [s^{-2}]

quality is gradually deteriorating, and their tendency of polluting the environment is becoming increasingly alarming. The disposal of radioactive waste is a point of concern in using nuclear energy. In the available renewable energy resources, biomass becomes an interesting choice (McKendry, 2002) and is expected to play a significant role in the future. Biomass conversion can be carried out through pyrolysis; a thermochemical decomposition at elevated temperatures in the absence of air, which is an efficient and an economical process of biomass conversion to gaseous fuel, liquid bio-oil, and solid biochar (Mettler et al., 2012). In order to better understand and improve the pyrolytic conversion process, it is important to know the thermal behaviour of biomass and the role of biomass constituents. Thermogravimetric analysis (TG), a thermal analysis technique, is often used for the thermal degradation studies (White et al., 2011). In TG, changes in the mass as a function of temperature and/or time are recorded, which is essential in calculating the kinetic parameters of the solid-state reactions. Model-free and model-fitting methods are often used to quantitatively describe the pyrolytic kinetics of the biomass (Cai et al., 2013; White et al., 2011). Although iso-conversional (model-free) methods provide accurate estimations of kinetic parameters without the knowledge of reaction mechanism, their applicability lacks in biomass conversions where overlapping devolatilizations, secondary reactions, diffusion, and catalytic effects further adds to the complexity (Hu et al., 2015). The heterogeneous biomass degradation involves more than one reaction (White et al., 2011) and for lignocellulosic biomass three independent-parallel-reactions (IPR) corresponding to the thermal decomposition of three pseudo-components are often considered (Anca-Couce, 2016). The three components are pseudo-hemicellulose (P-H), pseudo-cellulose (P-C), and pseudo-lignin (P-L). In some of the studies, activation energies (E_a) of the three pseudo-component were compared with the corresponding model compounds (Aboyade et al., 2011; Grønli et al., 1999), whereas others questioned the lignocellulosic structure made from the mixture of model compounds rather than using extracted constituents (Carrier et al., 2016; Gašparovič et al., 2012; Lv et al., 2010; Orfão et al., 1999). Although studies have recognised the importance of pseudo-components, research has yet to systematically investigate their role in the pyrolytic conversion of biomass.

Among various biomass resources, coconut shell waste (CSW) is the widely available lignocellulosic material in tropical regions of the world (Harries, 1978). It is mainly composed of lignin, cellulose, and hemicellulose (Rodrigues and Pinto, 2007). The pyrolysis process of the CSW consist of three stages of dehydration, degradation, and pyro-condensation (Gao et al., 2016). There is little published information on the kinetics of the CSW pyrolysis. Bandyopadhyay et al. (1999) carried out pyrolysis of the CSW in a tube furnace at 13 °C · min^{-1} and estimated the E_a ranging between 58.9 kJ.mol^{-1} and 114.8 kJ.mol^{-1} by considering two parallel reactions of first order. Tsamba et al. (2006) conducted a kinetics study of the CSW pyrolysis in a thermogravimetric analyzer (TGA) using heating rates of 5 °C · min^{-1} to 50 °C · min^{-1} and found E_α to vary from 179.6 to 216 kJ.mol^{-1} using the Coats and Redfern method considering two-parallel-reactions of first order. The latter study mentioned the E_α of P-H and P-C but the role of P-L was not examined. To the best of authors' knowledge, no previous study compared the model-free and the model-fitting methods for the CSW pyrolysis. In this study, the evolution of apparent E_α as a function of conversion, the reaction mechanism and the role of pseudo-components in the thermal degradation of the CSW during slow pyrolysis are investigated. This kinetics study will be helpful in understanding the conversion process and designing efficient pyrolyzers (Di Blasi, 2008; Papadikis et al., 2009) for the CSW pyrolysis.

2. Materials and methods

2.1. Lignocellulosic biomass

Whole coconut (Cocos nucifera) of the Indian origin was obtained from the local fruit market of Rabigh, Saudi Arabia. Coconut shell waste (CSW) was separated from the inner fruit and the

outer husk. The CSW was air-dried, crushed and ground in a hammer mill. A powder, with a particle size of less than 0.149 mm in accordance to Tyler standard sieves (i.e., 100% particles passed through 100 mesh screen) was preserved in an airtight jar for further characterization.

2.2. Physicochemical characterization

The amount of moisture, volatile matter and ash content of the CSW powder were determined according to E1756, E1755-01 and D3174-12 ASTM standard methods, respectively. The fixed carbon content was obtained from difference calculation (Basu, 2013). All measurements of the proximate analysis were performed three times and the average value with standard error are reported. The elemental analysis of the CSW powder was performed on CHN/O 2400 series II PerkinElmer, elemental analyzer.

2.3. Thermogravimetric analysis

The pyrolysis of the CSW powder was carried out in the TGA 4000 (Perkin Elmer Inc., Wellesley, MA, USA). An inert environment for pyrolysis was maintained by purging 20 mL · min^{-1} pure nitrogen gas, which was purchased from Abdullah Hashim Gas Company, Saudi Arabia. Approximately 35 ± 5 mg of the samples were loaded in an alumina pan and were subjected to heating from 40 to 995 °C at 10, 15 and 20 °C · min^{-1}, separately. An additional isothermal step before and after the constant heating rate was added to ensure stabilization before the start and at the end of the pyrolysis. The thermal analysis was performed on Pyris™ software. Each TG run was repeated twice to ensure accuracy and precision. The TG measurements were repeated three times only when the difference in the conversion was over 5% or the data were noisy. An advantage of a non-isothermal constant heating rate experiment is that the temperature range of interest can be investigated in a single run.

2.4. Kinetic theory

The kinetic parameters of biomass pyrolysis can be calculated assuming a simplified single-step global reaction mechanism (Eq. (1))

$$Biomass(s) \rightarrow Volatiles(g) + Biochar(s) \tag{1}$$

This reaction can be described by the rate equation according to Arrhenius law as

$$\frac{d\alpha}{dt} = A \cdot \exp\left(-\frac{E_a}{RT}\right) \cdot f(\alpha) \tag{2}$$

where α, R, A, E_a and $f(\alpha)$ denote the extent of conversion, the universal gas constant, pre-exponential factor, activation energy and the reaction model, respectively.

The extent of conversion or fraction of material converted during pyrolysis can be represented as Eq. (3).

$$\alpha = \frac{m_o - m_i}{m_o - m_f} \tag{3}$$

where m_0 is the initial mass, m_i is the instantaneous mass and m_f is the final mass after pyrolysis.

Commonly, the TG experiment is performed at a constant heating rate (β) i.e., the temperature (T) changes linearly with time (t) as in Eq. (4).

$$\beta = \frac{dT}{dt} \tag{4}$$

For a constant heating rate, Eq. (2) can be modified to Eq. (5).

$$\beta \frac{d\alpha}{dT} = A \cdot \exp\left(-\frac{E_a}{RT}\right) \cdot f(\alpha) \tag{5}$$

Integration with respect to temperature yields Eq. (6).

$$g(\alpha) = \int_0^{\alpha} \frac{d\alpha}{f(\alpha)} = \frac{A}{\beta} \int_0^{T} \exp\left(-\frac{E_a}{RT}\right) dT \tag{6}$$

This equation applies to the decomposition process, where the difference in the temperatures of the sample and the reference is insignificant.

2.4.1. Iso-conversional methods

Iso-conversional method derives its name from the fact that the reaction model $[f(\alpha)]$ at each conversion degree (α_i) of a particular heating rate (β_i) is constant. These methods are categorized as model-free methods which do not require any prior knowledge of the reaction model (Vyazovkin, 2006). The Friedman method (Friedman, 1964) is the most commonly used differential solution of Eq. (2). It is based on Eq. (7).

$$\ln\left(\frac{d\alpha}{dt}\right)_{\alpha_i} = \ln[A_\alpha \cdot f(\alpha)] - \frac{E_\alpha}{R \cdot T_{\alpha_i}} \tag{7}$$

where $\left(\frac{d\alpha}{dt}\right)_{\alpha_i}$, A_α, E_α and T_{α_i} denote the rate of conversion, the pre-exponential factor, the activation energy and the temperature at a particular conversion (α_i), respectively. The slope of the linear-fit of the graph between $\ln\left(\frac{d\alpha}{dt}\right)_{\alpha_i}$ and $\frac{1}{T_{\alpha_i}}$ gives $-\frac{E_\alpha}{R}$.

Despite being susceptible to data noise, the iso-conversional differential methods are helpful in predicting the kinetic parameters (Sbirrazzuoli et al., 1995). The shape of the differential thermogravimetric curves (DTG) or $\left(\frac{d\alpha}{dt}\right)$ vs temperature curves give useful information about the mechanism of the degradation i.e., if the process is based on a single reaction or multiple reactions (Aboyade et al., 2011; Mamleev et al., 2006).

The integral solution of Eq. (6) proposed by Flynn-Wall-Ozawa (FWO) (Flynn and Wall, 1966) is shown in Eq. (8).

$$\ln \beta_i = \text{const} - 1.052\left(\frac{E_\alpha}{R \cdot T_{\alpha_i}}\right) \tag{8}$$

The E_α is obtained from the slope of the linear regression fit of the plot between $\ln \beta_i$ and $\frac{1}{T_{\alpha_i}}$.

The Kissinger-Akahira-Sunose (KAS) integral solution (Akahira and Sunose, 1971) of Eq. (6) provides more accurate E_α values compared to FWO (Starink, 2003) and it is represented by linear Eq. (9).

$$\ln\left(\frac{\beta_i}{T_{\alpha_i}^2}\right) = \text{const} - \frac{E_\alpha}{R \cdot T_{\alpha_i}} \tag{9}$$

The slope of the linear fit of the $\ln\left(\frac{\beta_i}{T_{\alpha_i}^2}\right)$ vs $\frac{1}{T_{\alpha_i}}$ graph is used to estimate the apparent E_α.

The Kissinger method (Kissinger, 1957) is the commonly used solution of Eq. (6) under the condition of maximum conversion rate, as shown in Eq. (10).

$$\ln\left(\frac{\beta_i}{T_{p_i}^2}\right) = \ln\left[-\left(\frac{A_\alpha \cdot R}{E_a}\right) \cdot f'(\alpha)\right] - \frac{E_a}{R \cdot T_{p_i}} \tag{10}$$

where T_{p_i} and $f'(\alpha)$ are the peak-maximum temperature at a maximum conversion rate $\left(\frac{d\alpha}{dt}\right)_{p_i}$ of a particular heating rate (β_i) and the reaction model, respectively. The average E_a is estimated from the slope of the linear fit line of a graph between $\ln\left(\frac{\beta_i}{T_{\alpha_i}^2}\right)$ and $\frac{1}{T_{p_i}}$.

2.4.2. Model-fitting method

2.4.2.1. Single-step combined kinetics. The reaction mechanism can be described by a Šesták and Berggren (SB) model (Šesták and Berggren, 1971) as Eq. (11).

$$f(\alpha) = (1-\alpha)^n \cdot \alpha^m \cdot [-\ln(1-\alpha)]^p \tag{11}$$

where n m , and p are constant parameters.

Using the SB model, Eq. (2) can be transformed into Eq. (12).

$$\frac{d\alpha}{dt} = A \cdot \exp\left(-\frac{E_a}{RT}\right) \cdot (1-\alpha)^n \cdot \alpha^m \cdot [-\ln(1-\alpha)]^p \tag{12}$$

The SB model parameters can be estimated by minimizing the objective function (OF) through non-linear least square method using initial guess values of A and average E_a. This can be achieved through the Generalized Reduced Gradient (GRG) algorithm available in Microsoft Office Excel Solver.

$$OF = \sum \left(\left.\frac{d\alpha}{dt}\right|_{exp} - \left.\frac{d\alpha}{dt}\right|_{pred} \right)^2 \tag{13}$$

where $\left.\frac{d\alpha}{dt}\right|_{exp}$ and $\left.\frac{d\alpha}{dt}\right|_{pred}$ are the experimental and predicted conversion rates, respectively.

The quality of the model-fit can be determined in terms of fit (%) as Eq. (14)

$$Fit(\%) = \left(1 - \frac{\sqrt{\overline{OF}}}{\left(\left.\frac{d\alpha}{dt}\right|_{exp}\right)_p}\right) \times 100 \tag{14}$$

where $\overline{OF}$ is the average of the objective function and $\left(\left.\frac{d\alpha}{dt}\right|_{exp}\right)_p$ is the peak maximum value of the degradation rate.

2.4.2.2. Independent parallel reactions. In the literature, many studies describe pyrolysis of lignocellulosic biomass as a simplified single-step global reaction mechanism by Eq. (1) whereas others suggest multiple reaction mechanism to be suited for the complex biomass degradation. They proposed multiple reactions in parallel or in series (Anca-Couce et al., 2014; Manyà et al., 2003; Orfão et al., 1999).

Biomass constituents play their part in the thermochemical conversion. The constituents having similar structures degrade at similar temperatures so it is better to use the term pseudo-components. The pyrolysis, thus can be considered to consist of independent-parallel-reactions (IPR) of pseudo-components as described in Eq. (15).

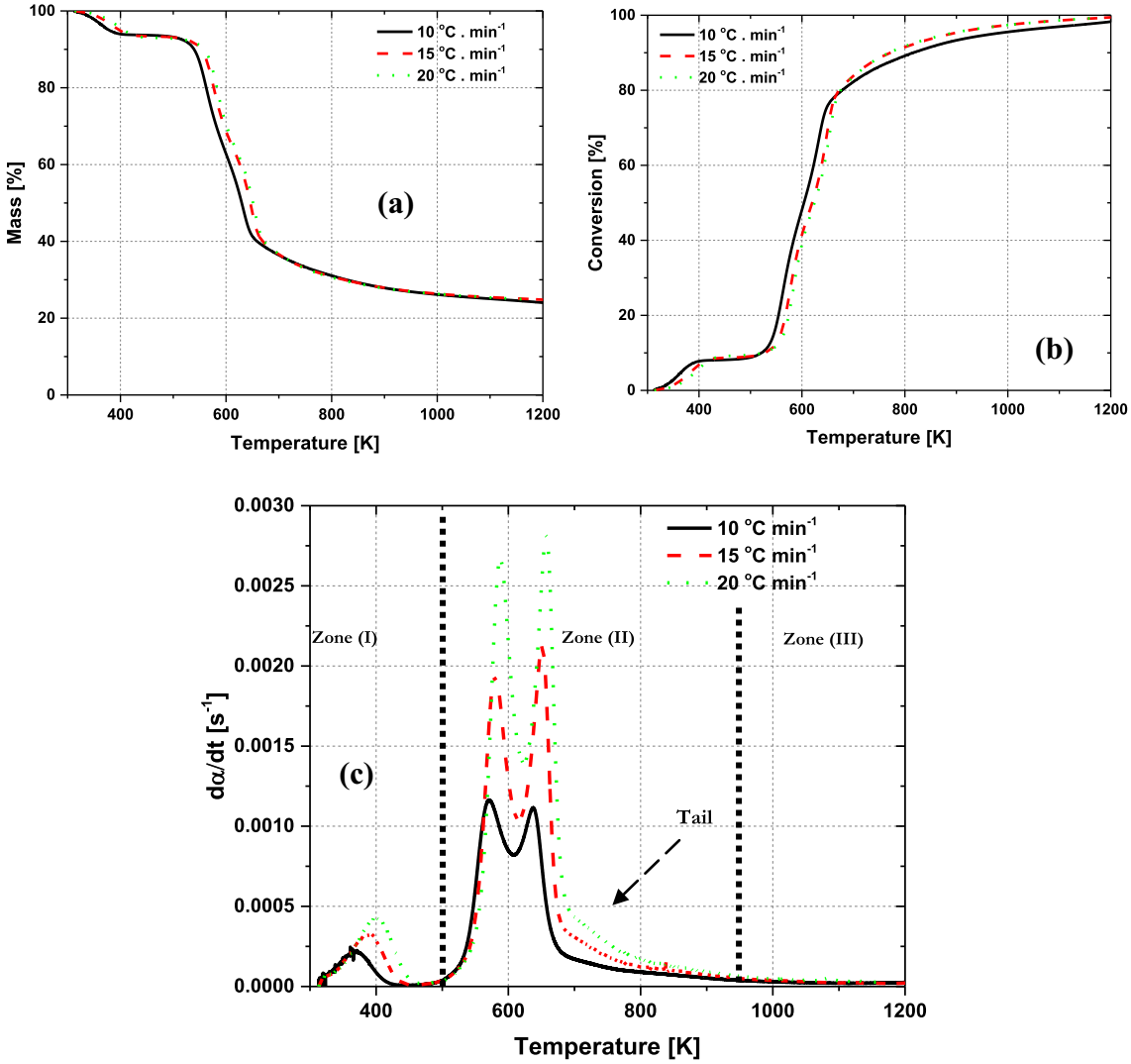

Fig. 1. a) Mass loss (%); b) Conversion degrees; and c) DTG curves of degradation at 10 °C · min^{-1}, 15 °C · min^{-1} and 20 °C · min^{-1}; zone (I) corresponds to initial devolatilization, zone (II) to the main decomposition and zone (III) to the pyrocondensation and carbonization.

$$\left.\begin{array}{ll}\text{Pseudo}-\text{component 1} & \xrightarrow{\frac{d\alpha_1}{dt}}\\ \text{Pseudo}-\text{component 2} & \xrightarrow{\frac{d\alpha_2}{dt}}\\ \text{Pseudo}-\text{component 3} & \xrightarrow{\frac{d\alpha_3}{dt}}\\ \vdots & \\ \text{Pseudo}-\text{component } N & \xrightarrow{\frac{d\alpha_N}{dt}}\end{array}\right\} \textit{Volatiles} + \textit{Biochar} \quad (15)$$

These pseudo-components degrade at specific temperatures and rates during pyrolysis. The rate of degradation of a pseudo-component can be described separately by Eq. (2), and the overall degradation rate can be obtained by summation as Eq. (16).

$$\frac{d\alpha}{dt} = \sum_{i=1}^{N}\frac{d\alpha_i}{dt} = \sum_{i=1}^{N}\gamma_i \cdot A_i \cdot \exp\left(-\frac{E_{ai}}{RT}\right)\cdot f(\alpha) \quad (16)$$

where N is the number of pseudo-components present in the biomass.

The modelled DTG curves can be obtained by adding pseudo-component degradation peaks through the nonlinear peak fitting tool of Origin® version 9.3 Pro using the Levenberg-Marquardt algorithm (LMA). The mass loss contribution (γ_i) is defined as the relative fraction of the area under the deconvoluted pseudo-component degradation peak. The quality of the fit can be assessed by correlation coefficient (R^2) and reduced chi-square value (χ^2_{red}) as shown in Eq. (17).

$$\chi^2_{red} = \frac{1}{\vartheta}\sum\frac{\left(\frac{d\alpha}{dt}\Big|_{exp} - \frac{d\alpha}{dt}\Big|_{pred}\right)^2}{\sigma^2} \quad (17)$$

where ϑ is the degree of freedom and σ^2 is the variance.

3. Results and discussions

3.1. Physico-chemical properties

The CSW used in this study contained 37.22% of carbon, 6.91% hydrogen, and 0.24% of nitrogen. The proximate composition of the CSW was 68.8 ± 1.5% of volatile matter, 19.7 ± 1.3% of fixed carbon, 3.6 ± 0.8% of ash, and 7.9 ± 1.1% of moisture. The amount of volatile matters present in the CSW was higher than the typical amount present in coal i.e., 12.2–44.5% (Vassilev et al., 2015). The ash content of the CSW is intermediate between wood-based and marine biomass. Typical ash content values reported in the literature for wood-based and marine biomass lies between 0.43% to 1.82% (Misra et al., 1993) and 6.46% to 27.24% (Wu et al., 2014), respectively. The amount of ash in softwood is comparatively higher than in the hardwood (Kim et al., 2010; Park et al., 2009). The H/C and C/N molar ratios of the CSW were found to be 2.2 and 180, respectively. Higher C/N molar ratio is essential for clean fuel combustion.

The potential energy content of a biomass is normally described by higher heating value (HHV). HHV of the CSW were determined from the ultimate and proximate compositions (Yin, 2011) as

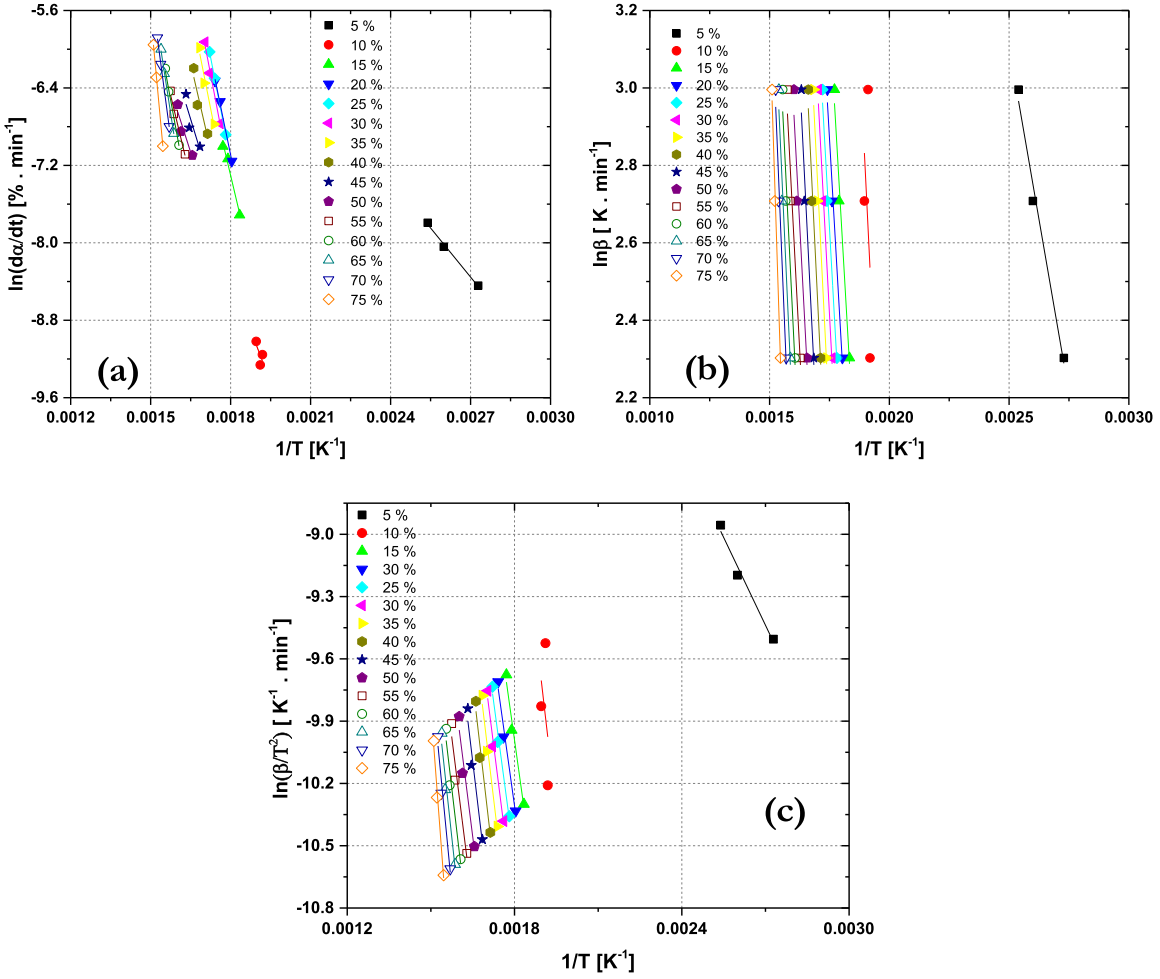

Fig. 2. Typical linear least square regression lines of iso-conversional methods at different conversions for (a) Friedman; (b) FWO; (c) KAS methods using TG data shown in Fig. 1.

18.1 MJ·kg^{-1} and 16.7 MJ·kg^{-1}, respectively. These HHV are in close agreement with the previously reported values for the CSW pyrolysis i.e., 17 MJ·kg^{-1} (Said et al., 2015) and 20.5 MJ·kg^{-1} (Tsamba et al., 2006). Compared to the HHV of coal i.e., 30 MJ·kg^{-1} (Channiwala and Parikh, 2002), the HHV of CSW is quite low. The higher content of volatiles and C/N molar ratio make CSW an interesting candidate feed-stock for biomass conversion through pyrolysis.

3.2. Kinetic analysis

The TG curves of CSW at different heating rates are shown in Fig. 1. Fig. 1(a–c) show mass loss, conversion, and DTG curves of the CSW as a function of temperature at constant heating rates of 10, 15 and 20 °C · min^{-1} in the temperature range of 300–1200 K. The DTG curves provide important information regarding the thermo-physical characteristics of the CSW. These curves can be divided into three zones. Initial devolatilization takes place in the zone I until 500 K. The main degradation of CSW takes place in zone II, extending from 500 to 950 K; the curve has a tail at around 700 K. It is an active pyrolysis zone where the degradation of biomass components (P-H, P-C, and P-L) take place. Almost about 60% of the total mass loss took place in this zone. The first peak in zone II corresponds to the degradation of P-H, followed by the second peak of P-C decomposition, whereas the tail is due to the decomposition of P-L. The peak of P-L is short, extending over a wider temperature range, and is fully overlapped by P-H and P-C degradation peaks. The overlapping peaks in the active pyrolysis zone indicate that the degradation is taking place through parallel reactions. The third zone is attributed to the pyro-condensation and carbonization (Gao et al., 2016). The shifting of the peaks laterally towards higher temperature and the increase in the degradation rate with the increase in the heating rate can be attributed to the improved transport phenomena (Asadieraghi and Wan Daud, 2014). This behaviour is more likely caused by the increase in the heat transfer rate from the surrounding to the sample (Caballero et al., 1997).

3.2.1. Iso-conversional methods

In Fig. 2, the linear regression lines of iso-conversional methods are fitted in the conversion range of 5–75% with a step size of 5%. The apparent E_α were estimated from the slopes of the regression lines of different iso-conversional methods and are reported in Table 1. The quality of fitted lines was assessed in terms of R^2. The R^2 values at 10% and at 80% and above for iso-conversional methods were low, hence the apparent E_α values calculated at these conversions were not accurate. These values were excluded from the calculation of average E_a in Table 1 and the corresponding data points are not shown in Fig. 6(b). Activation energy (E_a) by definition is the minimum energy required to initiate a reaction, it can also be used as a measure of the reactivity of a component. The average E_a of CSW estimated from iso-conversional methods varied between 94.7 and 126.6 kJ.mol^{-1}. These values are intermediate between 59.12 kJ.mol^{-1} and 179.6–216 kJ.mol^{-1} reported by Rakesh and Stewart (1986) and Tsamba et al. (2006), respectively.

Apparent activation energy (E_a) estimated from Friedman method is higher than FWO and KAS. The lower R^2 value at higher conversions can be attributed to the slow secondary reactions, non-uniform diffusion, and catalysis due to metals (Anca-Couce et al., 2014; Wang et al., 2016). The biochar formed at higher conversion possesses a porous structure due to which the rate of diffusion is increased. The volatiles can escape easily through the porous structure (Patnaik and Goldfarb, 2016) and the metals from the ash catalyze the degradation reaction thereby reducing the activation energy.

Table 1
Apparent activation energies, E_α[kJ · mol^{-1}] during the course of pyrolysis from Fig. 2.

Conversion [%]	Friedman (R^2)	FWO (R^2)	KAS (R^2)
2.5	26.8 (1.00)	28.1 (0.99)	23.6 (0.98)
5.0	28.1 (0.99)	28.3 (0.99)	23.4 (0.98)
7.5	61.8 (0.99)	39.7 (0.99)	35.0 (0.99)
12.5	77.6 (0.96)	91.5 (0.97)	87.2 (0.97)
15.0	96.8 (0.98)	84.8 (0.98)	80.0 (0.98)
17.5	105.8 (0.99)	84.3 (0.98)	79.4 (0.98)
20.0	111.2 (1.00)	85.2 (0.99)	80.2 (0.98)
22.5	115.4 (1.00)	86.7 (0.99)	81.7 (0.98)
25.0	117.7 (1.00)	88.5 (0.98)	83.5 (0.98)
27.5	119.3 (1.00)	90.7 (0.98)	85.8 (0.98)
30.0	119.9 (0.99)	93.0 (0.98)	88.2 (0.98)
32.5	118.8 (0.98)	95.5 (0.98)	90.8 (0.98)
35.0	115.7 (0.96)	98.0 (0.98)	93.3 (0.97)
37.5	109.4 (0.93)	100.0 (0.98)	95.4 (0.97)
40.0	99.4 (0.90)	101.2 (0.97)	96.6 (0.97)
42.5	87.3 (0.84)	100.7 (0.97)	95.9 (0.96)
45.0	74.9 (0.80)	98.7 (0.96)	93.8 (0.95)
47.5	69.0 (0.81)	96.0 (0.95)	90.8 (0.94)
50.0	71.5 (0.88)	93.8 (0.95)	88.5 (0.94)
52.5	81.0 (0.94)	93.2 (0.95)	87.7 (0.94)
55.0	95.6 (0.98)	94.6 (0.96)	89.1 (0.95)
57.5	111.3 (0.99)	97.2 (0.96)	91.8 (0.95)
60.0	125.3 (0.98)	100.5 (0.96)	95.2 (0.95)
62.5	137.6 (0.98)	104.3 (0.97)	99.1 (0.96)
65.0	149.1 (0.98)	108.6 (0.97)	103.6 (0.96)
67.5	160.5 (0.98)	113.6 (0.97)	108.8 (0.97)
70.0	172.4 (0.98)	119.8 (0.98)	115.3 (0.97)
72.5	192.4 (0.99)	129.5 (0.98)	125.4 (0.98)
75.0	246.8 (0.99)	152.1 (0.99)	149.1 (0.99)
77.5	599.4 (0.99)	278.3 (0.99)	281.7 (0.98)
Average (±SE) [kJ.mol^{-1}]	126.6 (±18.2)	99.2 (±7.7)	94.7 (±7.9)

3.2.2. Model-fitting methods

3.2.2.1. Single-step combined kinetics. Using the average E_a and A obtained from the differential (Friedman method) or integral (KAS method) iso-conversional methods, the SB model parameters were estimated by optimizing Eq. (12). The parameter values along with the OF values calculated from Eq. (13) are summarized in Table 2.

The parameters; n, m and p denote the reaction order, the power law, and the nucleation mechanisms, respectively. The average values of these parameters obtained from multiple heating rates can better describe the pyrolysis process (Sánchez-Jiménez et al., 2014) and can be represented by rate Eq. (18) using estimated average E_a and A from differential method.

$$\frac{d\alpha}{dt} = 2.09 \times 10^9 \cdot \exp\left(-\frac{126589}{RT}\right) \cdot (1-\alpha)^{4.6} \cdot [-\ln(1-\alpha)]^{0.2} \quad (18)$$

The rate law for the pyrolysis of CSW using the estimated average E_a and A from integral method is represented by Eq. (19)

$$\frac{d\alpha}{dt} = 3.44 \times 10^6 \cdot \exp\left(-\frac{94967}{RT}\right) \cdot (1-\alpha)^{4} \cdot [-\ln(1-\alpha)]^{0.53} \quad (19)$$

The optimum value of parameter n greater than unity signifies that the solid-state pyrolysis process may be controlled by order-based nucleation and growth mechanisms, which is also evident from the non-zero positive value of parameter p. In this mechanism, the nucleus grows and degrades due to collisions (Poletto et al., 2012). With a zero value of parameter m, there seems no role of the power law mechanism. The comparison between the experimental and simulated SB model conversion curves at different heating rates is shown in Fig. 3. It can be seen from Fig. 3 that the single-reaction integral model-fit is better fitted than the differential model-fit. Miura and Maki et al. reported similar results and regarded integral method to be more accurate in the dis-

Table 2
The SB model parameters obtained after optimizing Eq. (12).

β [°C·min^{-1}]	Differential					Integral				
	m	n	p	OF [s^{-2}]	fit [%]	m	n	p	OF [s^{-2}]	fit [%]
10	0	4.94	1×10^{-7}	1.59×10^{-4}	78.8	0	4.33	0.41	1.15×10^{-4}	83.6
15	0	4.50	0.29	2.35×10^{-4}	85.3	0	3.95	0.60	2.09×10^{-4}	86.1
20	0	4.35	0.32	3.21×10^{-4}	85.0	0	3.77	0.58	2.84×10^{-4}	85.8
Average (±SE)	0	4.60 (±0.18)	0.20 (±0.10)	–	–	0	4.01	0.53	–	–

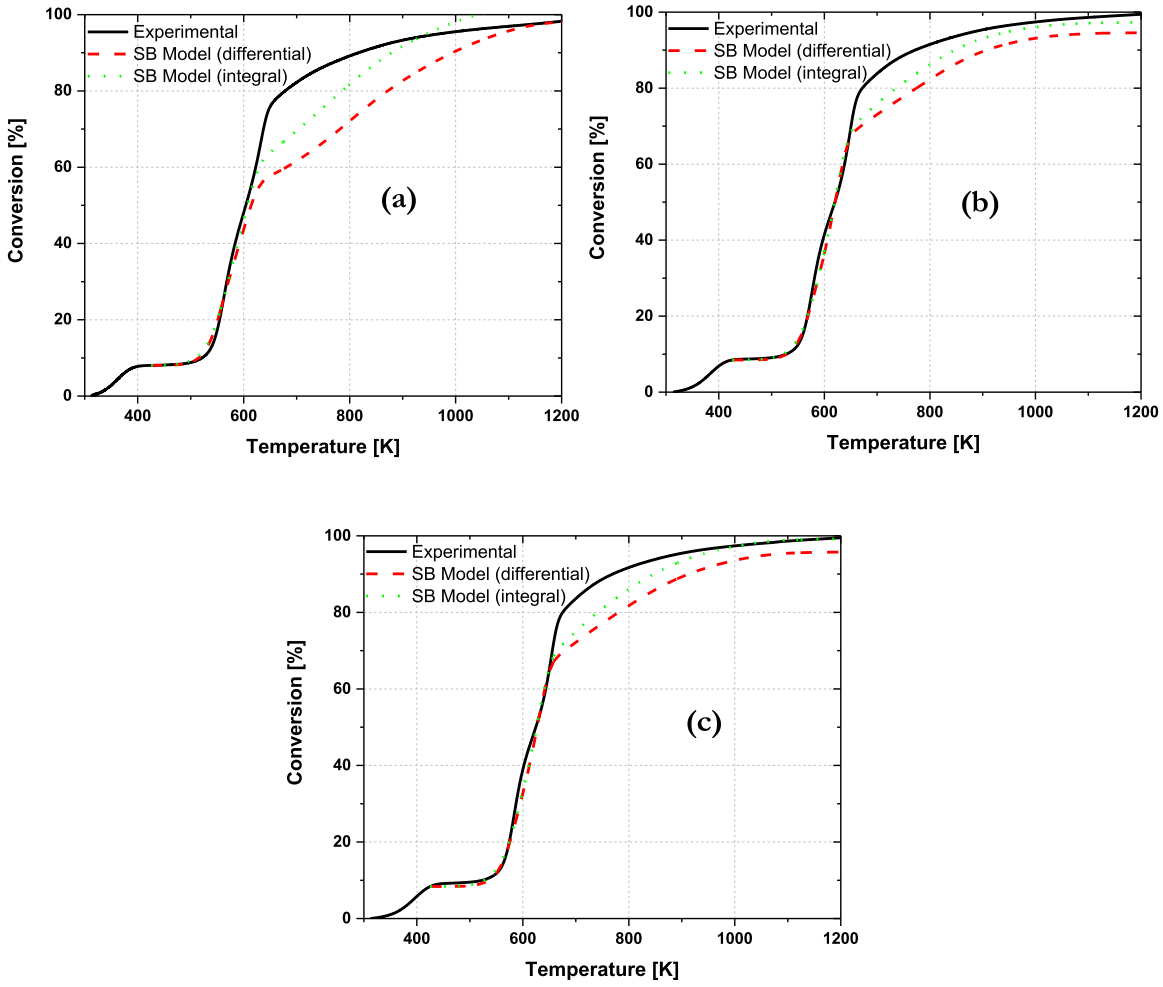

Fig. 3. Experimental and simulated conversion curves of coconut shell waste (CSW) at (a) 10 °C · min^{-1}; (b) 15 °C · min^{-1}; and (c) 20 °C · min^{-1} from Eq. (18).

tributed activation energy (DAEM) model-fitting method (Miura and Maki, 1998). At lower conversions, the predicted values are closer to the experimental data whereas the difference becomes significant at higher conversion levels. The disagreement at the higher conversions may have been caused by the multiple reactions occurring in the active pyrolysis zone.

3.2.2.2. Independent parallel reactions. Lignocellulosic biomass are mainly composed of hemicellulose, cellulose, and lignin. The shape of the DTG curvers in Fig. 1(c) with overlapping peaks suggest multiple reactions and it is reasonable to consider four parallel reactions corresponding to the degradations of four pseudo-component. The DTG curves were therefore, deconvoluted into four pseudo-components assuming Gaussian distributions at different heating rates as shown in Fig. 4.

Every deconvoluted DTG peak corresponds to a specific pseudo-component. These peaks were separated and are presented in Fig. 5.

It is apparent from Fig. 5, that the dehydration takes place in a narrow temperature range of 310–470 K. P-H degrades between 500 and 670 K with peak-maximum temperatures of 560–590 K depending on the heating rate. The degradation of P-C occurs between 550 and 720 K with peak-maximums centring around 630–660 K depending on the heating rate. These results are in good agreement with the previous reported temperature ranges for P-H and P-C decompositions (Kim et al., 2016, 2010; Orfão et al., 1999; Park et al., 2009). The degradation of P-L takes place in a wider temperature range of 450–950 K (Tsamba et al., 2006). However, the degradation rate of P-L was almost 5–6 times slower than the degradation rates of P-H and P-C. A likely possibility is that lig-

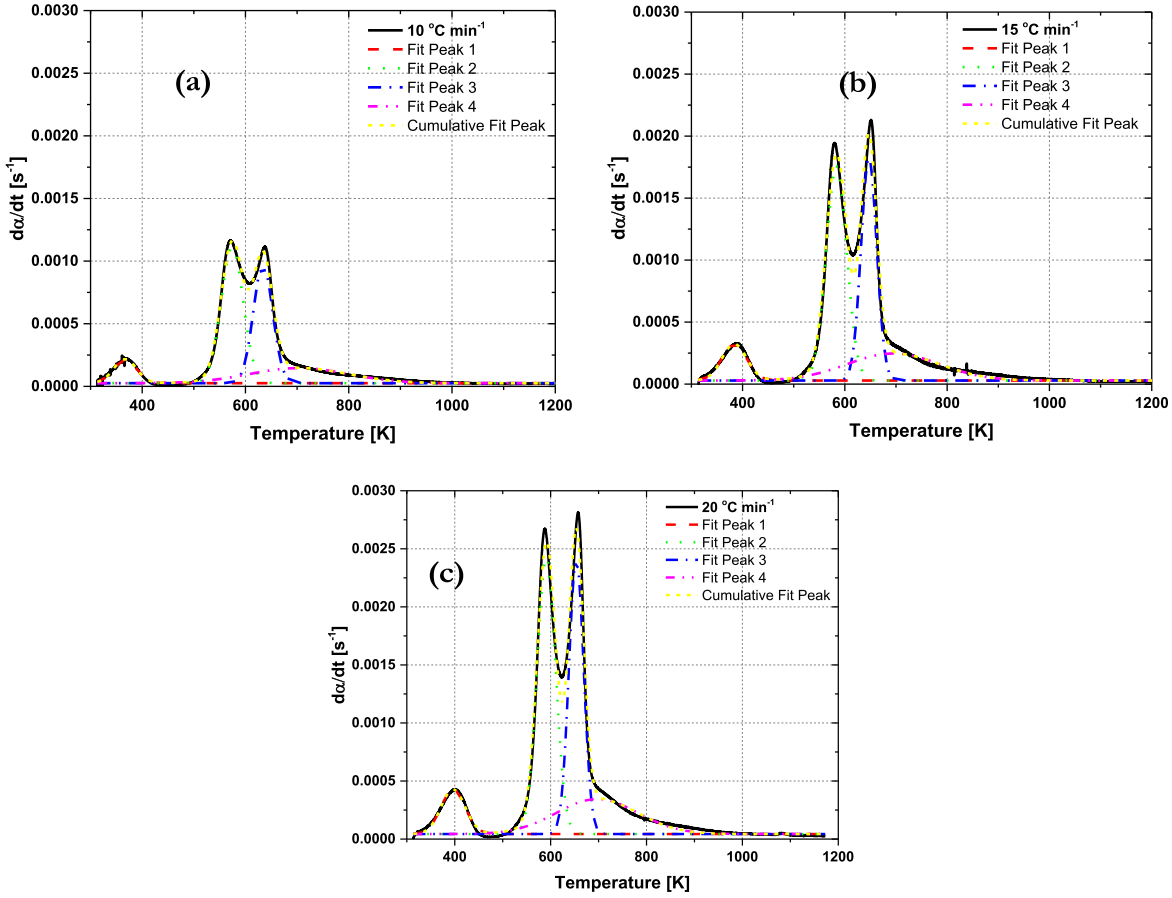

Fig. 4. Pseudo-components model-fitting of coconut shell waste (CSW) at (a) 10 °C · min^{-1}; (b) 15 °C · min^{-1}; and (c) 20 °C · min^{-1}.

nin is hindering the thermal decomposition process. The peak-maximum temperatures of the individual peaks at different heating rates were used to estimate the average E_a of pseudo-components according to Kissinger's method. Kissinger's plot is shown in Fig. 6(a). The E_a estimated from the slopes of linear data-fits in Fig. 6(a) are reported in Table 3.

R^2 value of P-L was lower than 0.8 so the estimated average E_a of P-L was considered inaccurate and hence not reported. The average E_a of P-W, P-H and P-C of the CSW estimated from the model-fitting method were 21.9, 106.4 and 108.6 kJ.mol^{-1}, respectively. Great variability in the E_a of the pseudo-components can be found in the published literature (Anca-Couce et al., 2014), which arise from many reasons like experimental and calculation errors, thermal lag, compensation effect, etc. (White et al., 2011). However, the average E_a of pseudo-components in lignocellulosic biomass do show a consistent trend; average E_a of P-H, P-C and P-L lies between 85 to 187 kJ.mol^{-1}, 80 to 249 kJ.mol^{-1} and 10 to 180 kJ.mol^{-1}, respectively (Tsamba et al., 2006; Aboyade et al., 2011; Anca-Couce, 2016). The estimated average E_a of the CSW pseudo-components corresponds well to the typical values of the lignocellulosic biomass. Fig. 6(b) compares the estimated apparent E_α from model-free and average E_α from model-fitting methods as a function of conversion. It is evident from Fig. 6(b) that the apparent E_α increased sharply at higher pyrolytic conversions. Water devolatilizes at lower temperature followed by the degradation of P-H and P-C with similar average E_a at near-temperature range. What stands out in this figure is the striking closeness of the average E_a of the pseudo-components to the apparent E_α obtained from FWO and KAS methods. Bartocci et al. (2017) reported similar coherence in the activation energy values of pseudo-components obtained from model-fitting and model-free methods. In other words, the average E_a activation energies of pseudo-components can be estimated with reasonable accuracy from the model-free methods provided the peak-maximum temperatures of the pseudo-components are known. P-L was found to be the most cumbersome for E_a calculations due to two main reasons, firstly due to its fully overlapped peak by P-H and P-C peaks and secondly due to its slow degradation rate; spanning over a wide range of temperature. Using average E_a and γ_i of other pseudo-components, the average E_a of P-L can be calculated from the weighted average as Eq. (20).

$$E_a = \frac{\sum \gamma_i E_{a_i}}{\sum \gamma_i} \tag{20}$$

Table 4 summarizes, the γ_i estimated for pseudo-component at different heating rates from the fractional area of the individual peak. The average γ_i of pseudo-water (P-W), P-H, P-C, and P-L were 7.9%, 39.5%, 31.1% and 21.5%, respectively. The E_a of P-L was estimated to be 79.7 and 228.5 kJ.mol^{-1} from Eq. (20) using average E_a of pseudo-components from Table 3, γ_i of pseudo-components from Table 4, and average E_a of pyrolysis from Table 1. The average E_a of P-L is consistent with the previous studies (Tsamba et al., 2006; Aboyade et al., 2011; Anca-Couce, 2016; Carrier et al., 2016). The variability of E_a of P-L indicates its structural heterogeneity and conversion to a highly cross-linked carbonaceous char (Sharma et al., 2004) during pyrolysis.

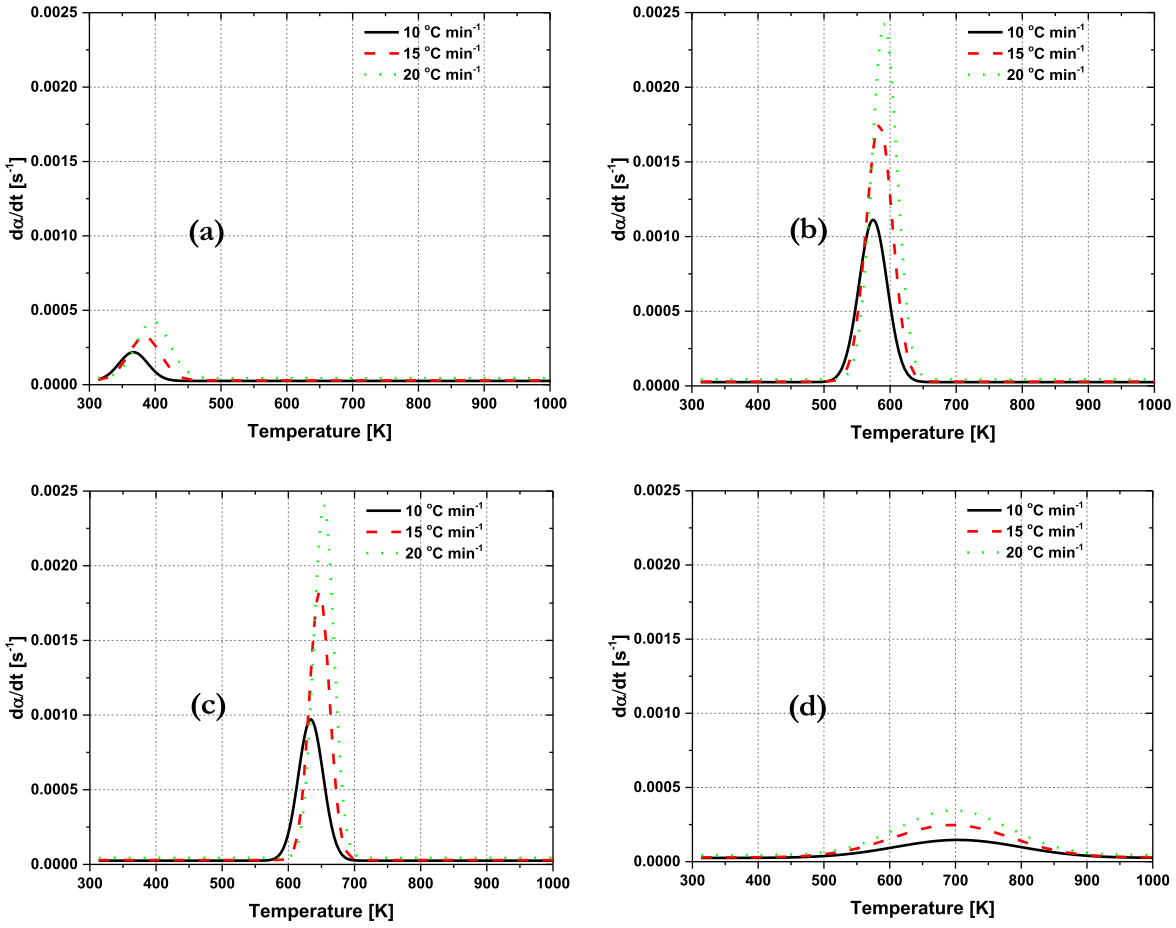

Fig. 5. DTG curves of pseudo-components of coconut shell waste (CSW) obtained by the deconvolution of global curves of Fig. 4; (a) Pseudo-water (P-W); (b) Pseudo-hemicellulose (P-H); (c) Pseudo-cellulose (P-C); (d) Pseudo-lignin (P-L).

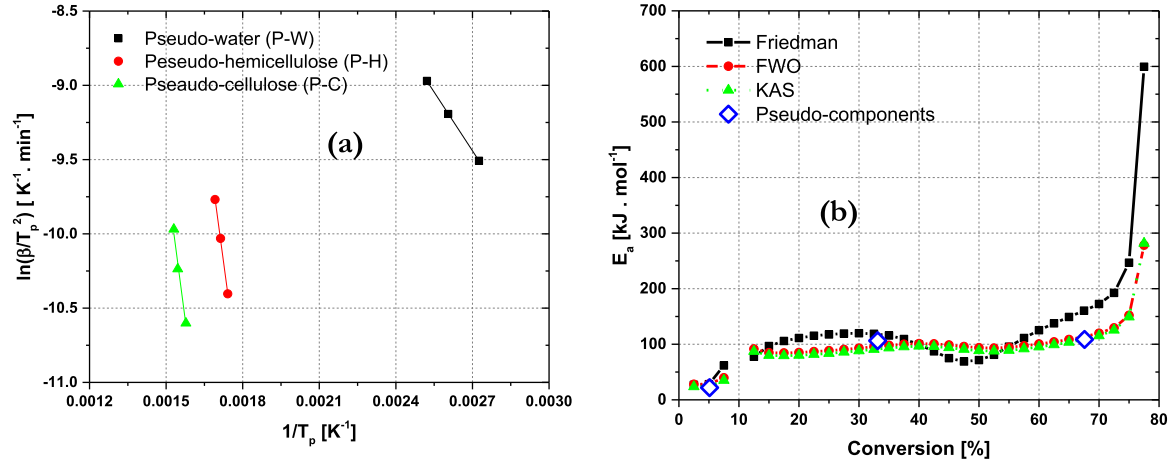

Fig. 6. a) Kissinger's plot of pseudo-components using T_p from Fig. 5; and b) Activation energies during the course of pyrolytic process from Tables 1 and 3.

Table 3
Average activation energies (E_a) of the pseudo-components present in CSW and their corresponding degradation temperatures.

Pseudo-components	Peak 1 (Pseudo-water, P-W)	Peak 2 (Pseudo-hemicellulose, P-H)	Peak 3 (Pseudo-cellulose, P-C)	Peak 4 (Pseudo-lignin, P-L)
Peak-Maximum Temperature (±SE) [K]	382.4 (±8.5)	583.1 (±4.8)	644.8 (±5.7)	698.5 (±2.6)
Conversion (±SE) [%]	5.1 (±0.1)	33.1 (±0.7)	67.6 (±0.3)	83.0 (±0.2)
Average activation Energy, $E_a(R^2)$ [kJ.mol^{-1}]	21.9 (1.00)	106.4 (0.99)	108.6 (0.98)	–

Table 4
Relative mass loss contributions (γ_i) of the pseudo-components obtained from Fig. 5.

Heating rate, β [°C·min^{-1}]	Pseudo-water, P-W	Pseudo-hemicellulose, P-H	Pseudo-cellulose, P-C	Pseudo-lignin, P-L	R^2	χ^2_{red}
10	0.075	0.408	0.312	0.204	0.995	3.86×10^{-10}
15	0.080	0.389	0.309	0.222	0.990	2.26×10^{-9}
20	0.083	0.389	0.310	0.218	0.991	3.90×10^{-9}
Average (±SE)	0.079 (±0.002)	0.395 (±0.006)	0.311 (±0.001)	0.215 (±0.005)	–	–

4. Conclusions

Order-based nucleation and growth mechanisms control the pyrolysis of coconut shell waste (CSW). The pyrolytic process of CSW can be kinetically described by four independent-parallel-reactions (IPR) each of which corresponds to a pseudo-component (pseudo-water, pseudo-hemicellulose, pseudo-cellulose and pseudo-lignin). Apparent activation energy was found to increase with the difficulty in decomposing complex pseudo-components with the progression of pyrolytic conversion. Average activation energies of dehydration, decomposition of pseudo-cellulose and pseudo-hemicellulose estimated from the model-fitting method were 21.9 kJ.mol^{-1}, 106.4 kJ.mol^{-1} and 108.6 kJ.mol^{-1}, respectively. These values correspond well to the apparent activation energies obtained from model-free methods which suggest that model-free methods can be used to estimate average activation energies of pseudo-components from their peak-maximum temperatures. Pseudo-cellulose and pseudo-hemicellulose degrade approximately 5–6 times faster than lignin.

References

Aboyade, A.O., Hugo, T.J., Carrier, M., Meyer, E.L., Stahl, R., Knoetze, J.H., Görgens, J.F., 2011. Non-isothermal kinetic analysis of the devolatilization of corn cobs and sugar cane bagasse in an inert atmosphere. Thermochim. Acta 517, 81–89.

Akahira, T., Sunose, T., 1971. Method of determining activation deterioration constant of electrical insulating materials. Res. Report Chiba Inst. Technol. (Sci. Technol.) 16, 22–31.

Anca-Couce, A., 2016. Reaction mechanisms and multi-scale modelling of lignocellulosic biomass pyrolysis. Progr. Energy Combust. Sci. 53, 41–79.

Anca-Couce, A., Berger, A., Zobel, N., 2014. How to determine consistent biomass pyrolysis kinetics in a parallel reaction scheme. Fuel 123, 230–240.

Asadieraghi, M., Wan Daud, W.M.A., 2014. Characterization of lignocellulosic biomass thermal degradation and physiochemical structure: effects of demineralization by diverse acid solutions. Energy Converse. Manage. 82, 71–82.

Bandyopadhyay, S., Chowdhury, R., Biswas, G.K., 1999. Thermal deactivation studies of coconut shell pyrolysis. Can. J. Chem. Eng. 77, 1028–1036.

Bartocci, P., Anca-Couce, A., Slopiecka, K., Nefkens, S., Evic, N., Retschitzegger, S., Barbanera, M., Buratti, C., Cotana, F., Bidini, G., Fantozzi, F., 2017. Pyrolysis of pellets made with biomass and glycerol: kinetic analysis and evolved gas analysis. Biomass Bioenergy 97, 11–19.

Basu, P., 2013. Chapter 3 – biomass characteristics. In: Biomass Gasification, Pyrolysis and Torrefaction. Academic Press, Boston, pp. 47–86.

Caballero, J.A., Conesa, J.A., Font, R., Marcilla, A., 1997. Pyrolysis kinetics of almond shells and olive stones considering their organic fractions. J. Anal. Appl. Pyrolysis 42, 159–175.

Cai, J., Wu, W., Liu, R., Huber, G.W., 2013. A distributed activation energy model for the pyrolysis of lignocellulosic biomass. Green Chem. 15, 1331–1340.

Carrier, M., Auret, L., Bridgwater, A., Knoetze, J.H., 2016. Using apparent activation energy as a reactivity criterion for biomass pyrolysis. Energy Fuels 30, 7834–7841.

Channiwala, S.A., Parikh, P.P., 2002. A unified correlation for estimating HHV of solid, liquid and gaseous fuels. Fuel 81, 1051–1063.

Di Blasi, C., 2008. Modeling chemical and physical processes of wood and biomass pyrolysis. Progr. Energy Combust. Sci. 34, 47–90.

Flynn, J.H., Wall, L.A., 1966. A quick, direct method for the determination of activation energy from thermogravimetric data. J. Polym. Sci. B Polym. Lett. 4, 323–328.

Friedman, H.L., 1964. Kinetics of thermal degradation of char-forming plastics from thermogravimetry. Application to a phenolic plastic. J. Polym. Sci. C Polym. Symp. 6, 183–195.

Gao, Y., Yang, Y., Qin, Z., Sun, Y., 2016. Factors affecting the yield of bio-oil from the pyrolysis of coconut shell. Springerplus 5.

Gašparoviè, L., Labovský, J., Markoš, J., Jelemenský, L., 2012. Calculation of kinetic parameters of the thermal decomposition of wood by distributed activation energy model (DAEM). Chem. Biochem. Eng. Q. 26, 45–53.

Grønli, M., Antal, M.J., Várhegyi, G., 1999. A round-robin study of cellulose pyrolysis kinetics by thermogravimetry. Ind. Eng. Chem. Res. 38, 2238–2244.

Harries, H.C., 1978. The evolution, dissemination and classification of Cocos nucifera L. Bot. Rev 44, 265–319.

Hu, M., Chen, Z., Guo, D., Liu, C., Xiao, B., Hu, Z., Liu, S., 2015. Thermogravimetric study on pyrolysis kinetics of Chlorella pyrenoidosa and bloom-forming cyanobacteria. Bioresour. Technol. 177, 41–50.

Kim, S.-S., Kim, J., Park, Y.-H., Park, Y.-K., 2010. Pyrolysis kinetics and decomposition characteristics of pine trees. Bioresour. Technol. 101, 9797–9802.

Kim, S.-S., Ly, H.V., Chun, B.H., Ko, J.-H., Kim, J., 2016. Thermogravimetric characteristics of α-cellulose and decomposition kinetics in a micro-tubing reactor. Korean J. Chem. Eng. 33, 3128–3133.

Kissinger, H.E., 1957. Reaction kinetics in differential thermal analysis. Anal. Chem. 29, 1702–1706.

Lv, G.-J., Wu, S.-B., Lou, R., 2010. Kinetic study of the thermal decomposition of hemicellulose isolated from corn stalk. BioResources 5, 1281–1291.

Mamleev, V., Bourbigot, S., Le Bras, M., Yvon, J., Lefebvre, J., 2006. Model-free method for evaluation of activation energies in modulated thermogravimetry and analysis of cellulose decomposition. Chem. Eng. Sci. 61, 1276–1292.

Manyà, J.J., Velo, E., Puigjaner, L., 2003. Kinetics of biomass pyrolysis: a reformulated three-parallel-reactions model. Ind. Eng. Chem. Res. 42, 434–441.

McKendry, P., 2002. Energy production from biomass (Part 2): conversion technologies. Bioresour. Technol. Rev. Issue 83, 47–54.

Mettler, M.S., Vlachos, D.G., Dauenhauer, P.J., 2012. Top ten fundamental challenges of biomass pyrolysis for biofuels. Energy Environ. Sci. 5, 7797–7809.

Misra, M.K., Ragland, K.W., Baker, A.J., 1993. Wood ash composition as a function of furnace temperature. Biomass Bioenergy Biomass Combust. Challenge Biomass? 4, 103–116

Miura, K., Maki, T., 1998. A simple method for estimating f(E) and k0(E) in the distributed activation energy model. Energy Fuels 12, 864–869.

Orfão, J.J.M., Antunes, F.J.A., Figueiredo, J.L., 1999. Pyrolysis kinetics of lignocellulosic materials—three independent reactions model. Fuel 78, 349–358.

Papadikis, K., Gu, S., Bridgwater, A.V., Gerhauser, H., 2009. Application of CFD to model fast pyrolysis of biomass. Fuel Process. Technol. 90, 504–512.

Park, Y.-H., Kim, J., Kim, S.-S., Park, Y.-K., 2009. Pyrolysis characteristics and kinetics of oak trees using thermogravimetric analyzer and micro-tubing reactor. Bioresour. Technol. 100, 400–405.

Patnaik, A.S., Goldfarb, J.L., 2016. Continuous activation energy representation of the Arrhenius equation for the pyrolysis of cellulosic materials: Feed corn stover and cocoa shell biomass. Cellulose Chem. Technol. 50, 311–320.

Poletto, M., Zattera, A.J., Santana, R.M.C., 2012. Thermal decomposition of wood: kinetics and degradation mechanisms. Bioresour. Technol. Adv. Biol. Waste Treat. Bioconversion Technol. 126, 7–12.

Rakesh, B.C.K., Stewart, D.F., 1986. An investigation of the kinetics of coconut shell pyrolysis. Resour. Conserv. 12, 137–139.

Rodrigues, S., Pinto, G.A.S., 2007. Ultrasound extraction of phenolic compounds from coconut (Cocos nucifera) shell powder. J. Food Eng. 80, 869–872.

Said, M., John, G., Mhilu, C., Manyele, S., 2015. The study of kinetic properties and analytical pyrolysis of coconut shells. J. Renew. Energy, 307–329.

Sánchez-Jiménez, P.E., Rodríguez-Laguna, M. del R., Pérez-Maqueda, L.A., Criado, J. M., 2014. Comments on "Pyrolysis kinetics of biomass from product information" (Applied Energy 110 (2013) 1–8) regarding the inability to obtain meaningful kinetic parameters from a single non-isothermal curve. Appl. Energy 125, 132–135.

Sbirrazzuoli, N., Girault, Y., Elégant, L., 1995. Simulations for evaluation of kinetic methods in differential scanning calorimetry. Part 1. Application to single-peak methods: Freeman-Carroll, Ellerstein, Achar-Brindley-Sharp and multiple linear regression methods. Thermochim. Acta 260, 147–164.

Šesták, J., Berggren, G., 1971. Study of the kinetics of the mechanism of solid-state reactions at increasing temperatures. Thermochim. Acta 3, 1–12.

Sharma, R.K., Wooten, J.B., Baliga, V.L., Lin, X., Geoffrey Chan, W., Hajaligol, M.R., 2004. Characterization of chars from pyrolysis of lignin. Fuel, Fundam. Mech. Biomass Pyrolysis Oxid. 83, 1469–1482.

Starink, M.J., 2003. The determination of activation energy from linear heating rate experiments: a comparison of the accuracy of isoconversion methods. Thermochim. Acta 404, 163–176.

Tsamba, A.J., Yang, W., Blasiak, W., 2006. Pyrolysis characteristics and global kinetics of coconut and cashew nut shells. Fuel Process. Technol. 87, 523–530.

Vassilev, S.V., Vassileva, C.G., Vassilev, V.S., 2015. Advantages and disadvantages of composition and properties of biomass in comparison with coal: an overview. Fuel 158, 330–350.

Vyazovkin, S., 2006. Model-free kinetics. J. Therm. Anal. Calorim. 83, 45–51.

Wang, X., Hu, M., Hu, W., Chen, Z., Liu, S., Hu, Z., Xiao, B., 2016. Thermogravimetric kinetic study of agricultural residue biomass pyrolysis based on combined kinetics. Bioresour. Technol. 219, 510–520.
White, J.E., Catallo, W.J., Legendre, B.L., 2011. Biomass pyrolysis kinetics: a comparative critical review with relevant agricultural residue case studies. J. Anal. Appl. Pyrolysis 91, 1–33.
Wu, K., Liu, J., Wu, Y., Chen, Y., Li, Q., Xiao, X., Yang, M., 2014. Pyrolysis characteristics and kinetics of aquatic biomass using thermogravimetric analyzer. Bioresour. Technol. 163, 18–25.
Yin, C.-Y., 2011. Prediction of higher heating values of biomass from proximate and ultimate analyses. Fuel 90, 1128–1132.